Carbohydrate Polymers 296 (2022) 119911

Contents lists available at ScienceDirect

Carbohydrate Polymers

journal homepage: www.elsevier.com/locate/carbpol

Rheology of concentrated and highly concentrated enzymatic cellulose nanofibril hydrogels during lubricated compression

F. Martoïa [a,*], S. Gupta [a,b], P.J.J. Dumont [a], L. Orgéas [b]

[a] Univ. Lyon, INSA-Lyon, CNRS, LaMCoS, UMR5259, 69621 Villeurbanne, France
[b] Univ. Grenoble Alpes, CNRS, Grenoble INP, 3SR Lab, F-38000 Grenoble, France

ARTICLE INFO

Keywords:
Cellulose nanofibrils
Flocculated hydrogels
Lubricated compression
Elongational flow
Segregation

ABSTRACT

Processing cellulose nanofibril (CNF) hydrogels with a high concentration is a solution to reduce logistics costs and drying energy and to produce CNF-based materials with good dimensional stability. However, the rheology of concentrated and highly concentrated CNF hydrogels is poorly understood due to the difficulties to characterise them using standard shear rheometers. In this study, enzymatic CNF hydrogels in the concentrated and highly concentrated regimes (3–13.6 wt%) were subjected to lubricated compression at various strain rates. At low strains, compression curves exhibited a linear regime. At higher strains and low strain rates, a heterogeneous and marked hardening of stress levels was observed and accompanied with a two-phase flow with significant fluid segregation and network consolidation. At high strain rates, a homogeneous and incompressible one-phase plateau-like regime progressively established. In this regime, a yield stress was measured and compared with literature data, showing a good agreement with them.

1. Introduction

Cellulose nanofibrils (CNFs) are the main elementary reinforcements of plant and wood cell walls (Dufresne, 2017). They are mainly extracted in the form of colloidal hydrogels (Nechyporchuk et al., 2016) at a concentration that classically ranges between 1 wt% and 3 wt%, using a mechanical disintegration process of the plant or wood fibres (Dufresne, 2017) (Klemm et al., 2018; Nechyporchuk et al., 2016). The mechanical process is often combined with enzymatic or chemical pre-treatments to reduce the input energy needed for the production of CNF hydrogels (Henriksson et al., 2007; Isogai et al., 2011; Pääkkö et al., 2007; Saito et al., 2007).

Depending upon the extraction route, the morphology (width, slenderness, tortuosity) and the physico-chemical surface properties (*e.g.*, surface charge density) of CNFs can significantly vary (Nechyporchuk et al., 2016). Mechanically and enzymatically treated CNF hydrogels are usually flocculated systems that contain a great amount of nanoscale elements in the form of fibril aggregates and residual microscale elements such as partially fibrillated fibres (Nechyporchuk et al., 2016). Typically, the diameter and length of nanoscale elements range from 5 to 100 nm and from 1 μm to 10 μm, respectively (Dufresne, 2017; Martoïa et al., 2015). Owing to their important aspect ratio (≈50–300), significant specific surface area (≈40–800 μm^{-1}), as well as their remarkable mechanical properties (longitudinal Young's modulus ≈90 GPa, longitudinal stress at break ≈0.5–1 GPa (Cheng et al., 2009; Moon et al., 2011)), CNFs constitute promising biosourced nanofibrous reinforcements that can be used as gelling agents for cosmetics (Meftahi et al., 2022), coating slurries for the papermaking industry (Lavoine et al., 2012; Li et al., 2021; Missoum et al., 2013), thickeners or emulsion stabilisers for the food industry (Gómez et al., 2016) or as building blocks to obtain filaments, films or nanopapers as well as foams or aerogels for a wide range of applications (Gupta et al., 2018; Liu et al., 2022; Lundahl et al., 2017).

During the processing of the aforementioned materials, CNF hydrogels are subjected to complex flow kinematics, including shear and elongational deformations (Hubbe et al., 2017; Wang et al., 2019). For instance, intense shear can occur during pumping and mixing operations (Hubbe et al., 2017), elongation during spinning and drawing operations related to the fabrication of continuous filaments (Kim et al., 2019; Lundahl et al., 2017), or compression during pressing and coating operations of films or nanopapers (Dimic-Misic et al., 2017; Rantanen et al., 2015) as well as during the solidification phase of the ice-templating processing route to produce CNF foams or aerogels (Gupta et al., 2018). To obtain CNF-based materials with optimised

* Corresponding author.
E-mail address: florian.martoia@insa-lyon.fr (F. Martoïa).

https://doi.org/10.1016/j.carbpol.2022.119911
Received 16 June 2022; Received in revised form 17 July 2022; Accepted 18 July 2022
Available online 26 July 2022

microstructures and end-use properties, it is crucial to control the rheology and related flow-induced nanostructures (*e.g.*, fibril orientation) and mesostructures (*e.g.*, evolution of the size and shape of flocs) of CNF hydrogels under various flow conditions.

The shear rheology of the mechanically and enzymatically treated CNF hydrogels has been studied extensively in the literature (Hubbe et al., 2017). The majority of the rheological studies are focused on CNF hydrogels with moderate CNC concentrations of 0.5–3 wt%, leading to semi-concentrated to concentrated systems. Only few shear rheological data have been reported for highly concentrated (up to 10 wt%) enzymatic CNF hydrogels (Jaiswal et al., 2021). However, this is of great interest since processing highly concentrated CNF hydrogels allows reducing the transportation and logistics costs, saving energy, reducing shrinkage during drying of CNF hydrogels and enhancing dimensional stability of CNF-based products (Sinquefield et al., 2020). All these studies have shown that CNF hydrogels exhibit an apparent yield-stress at low shear rates and a shear thinning behaviour at higher ones (Hubbe et al., 2017) (Koponen, 2020; Martoïa et al., 2015; Martoïa et al., 2016). At intermediate shear rates, their shear response is erratic. This particular behaviour is related to complex phenomena related to the aggregation and/or disaggregation of flocs, which evolve with the applied shear rate history (Karppinen et al., 2012; Martoïa et al., 2016; Saarikoski et al., 2012). Several studies have shown that shear tests are often affected by heterogeneous flow kinematics (*e.g.*, wall slippage, shear wall depletion, shear banding (Martoïa et al., 2015; Nechyporchuk et al., 2014; Saarinen et al., 2014)) that hinder the interpretation of the rheological data and question the relevance of these tests for CNF hydrogels. These problems are all the more prone to occur as the CNF concentration is increased (Nechyporchuk et al., 2015). To circumvent these difficulties, various observation techniques such as ultrasonic speckle velocimetry (Martoïa et al., 2015) or optical coherent tomography (Saarinen et al., 2014) have been used to better analyse the flow kinematics and extract relevant rheological parameters for CNF hydrogels.

Few studies in the literature are dedicated to the extensional rheology of CNF hydrogels. These experiments used devices based on the principle of capillary flow rheometer equipped with a convergent nozzle (Moberg et al., 2014) or capillary breakup extensional rheometer (Lundahl et al., 2018). Due to the complexity of these setups, the data obtained by these approaches are difficult to analyse. Even if the results are difficult to interpret, they tend to show an extensional thinning behaviour of the CNF hydrogels. However, the authors did not report any measurements of extensional yield stress for the studied CNF hydrogels. It is worth mentioning that for other concentrated fibrous and/or aqueous systems, lubricated compression was proved to be a suitable test to analyse their complex in-plane elongational flow (Chalencon et al., 2010; Guiraud et al., 2012; Le Corre et al., 2002; Meeten, 2002; Orgéas et al., 2008; Ovarlez et al., 2010).

In this context, we hypothesized that the extensional behaviour of concentrated and highly concentrated enzymatic CNF hydrogels (CNF concentration up to 13.6 wt%) can be thoroughly investigated using lubricated compression under various strain rates, so as various relevant elastoviscoplastic parameters can be identified. The used compression device was equipped with optical visualisation systems to observe and to better understand the complex flow of CNF hydrogels during compression.

2. Materials and methods

2.1. Materials

An enzymatic CNF hydrogel at a weight (resp. volume) concentration c (resp. ϕ_f) of 3 wt% (resp. 2 %) was supplied by Centre Technique du Papier (Grenoble, France). These CNF hydrogels were obtained from a birch bleached kraft pulp using a procedure briefly described hereafter. The pulp was slushed in a pulper and then transferred to a tank in which the enzymatic treatment was carried out. The fibres in water suspension (4 wt%) were hydrolysed under mild conditions (15 min, pH = 6, 50 °C) by adding 4 ml of endoglucanases (Novozym 476, Novozymes, Denmark) per kilogram of fibres (or conversely 20 U g^{-1}). The enzymatically-treated fibres were then extensively refined in disc refiners using a decreasing refining intensity from 0.5 J m^{-1} to 0.1 J m^{-1}. The suspension was then diluted to a concentration of 3 wt% and subjected to a second refining stage with a decreasing refining intensity from 0.1 J m^{-1} to 0.01 J m^{-1}. Then, the fibres were mechanically disintegrated using a homogeniser M-110 EH-30 (GEA Niro Soavi, Parma, Italy) at 1500 bar and 3 passes. Fig. 1a,b show SEM and TEM micrographs of a CNF film obtained after drying drops of diluted CNF hydrogel (Martoïa et al., 2016). These micrographs reveal that the CNF hydrogel contained microscale elements, *i.e.*, partially fibrillated fibres, and nanoscale elements in the form of cellulose fibril aggregates. The quantitative analysis of both SEM and TEM images was performed manually with ImageJ software (Schneider et al., 2012). This enabled the distributions for the widths of the microscale and nanoscale elements to be plotted in Fig. 1c, d, respectively. The microscale elements exhibited a mean width of $\overline{w} \approx 9.4$ μm and the nanoscale elements had a mean width $\overline{w} \approx 21.6$ nm. Due to the difficulty to distinguish individualised CNFs, it was not possible to measure with enough accuracy their lengths.

2.2. Concentration of CNF hydrogels

A specific methodology was developed to prepare CNF hydrogels at high weight (resp. volume) concentrations c (resp. ϕ_f) of 8 wt% (resp. 5.5 %) and 13.6 wt% (resp. 9.5 %) (Fig. 2). A mass m of 100 g of CNF hydrogel at the initial weight concentration was poured into a rectangular aluminium tray of 250 ml capacity and placed into a vacuum oven (Thermo scientific Heraeus, VT6060M) at a vacuum pressure p of 0.01 mbar and a temperature T of 50 °C. The hydrogel was taken out from the vacuum oven every 20 min and was homogenised with a disperser (IKA Ultra-Turrax T-18) at 3000 rpm. The drying and homogenisation process was repeated until reaching the desired concentrations c of 8 wt% and 13 wt%. The final hydrogel concentration c was checked using a gravimetric method.

2.3. Lubricated compression experiments

The rheology of concentrated and highly concentrated CNF hydrogels was studied using lubricated compression tests with cylindrical samples. The testing procedure was adapted from those reported in (Chalencon et al., 2010; Guiraud et al., 2012 and Le Corre et al., 2002) to characterise the complex in-plane elongational flows of concentrated fibre suspensions and granular systems. To prepare the samples, a mass of 10 g of CNF hydrogel was homogenised at 3000 rpm using the Ultra-Turrax disperser. To remove the air bubbles introduced during the mixing step, the CNF hydrogel samples were placed in vacuum at 0.01 mbar for a few minutes. A prescribed amount of CNF hydrogel was then poured into a cylindrical mould made of Teflon. Finally, the CNF hydrogel sample was removed carefully from the mould. The as-prepared samples were cylinders with an initial diameter $d_0 = 13.1$ mm, and an initial height $h_0 = 3.0$ mm. The lubricated compression experiments were performed using an electromechanical tension-compression machine (Shimadzu – AG-X with force sensor of 100 N) equipped with parallel square aluminium platens (25 mm in width) (Fig. 3a). Teflon sheets were stuck onto their surface. In addition, to avoid friction-induced shear effects, the platens were coated with silicone oil with a shear viscosity μ = 0.02 Pa s.

During the tests, the instantaneous height h and the compression force F were recorded. The CNF hydrogels at standard concentration (3 wt%) were compressed with constant compression velocities $\dot{h}$ that ranged from 0.2 to 150 mm min^{-1}, whereas the CNF hydrogels at 8 wt%

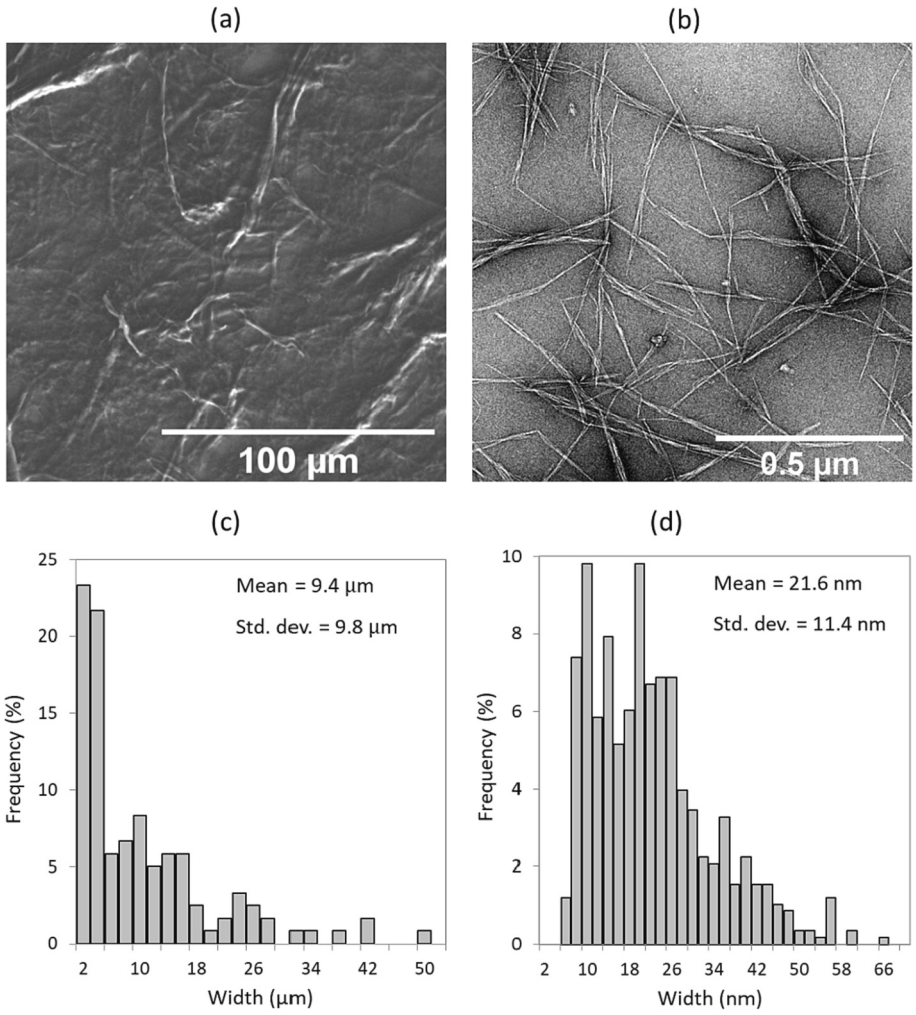

Fig. 1. (a) SEM micrograph of a film obtained after drying a CNF hydrogel that was diluted with distilled water at 0.1 wt%. (b) TEM micrograph of a film obtained after drying a CNF hydrogel that was diluted with distilled water at 0.001 wt%. (c) Width distribution of the microscale elements obtained from 100 measurements performed on 5 SEM micrographs. (d) Width distribution of the nanoscale fibril aggregates obtained from 100 measurements performed on 5 TEM micrographs.

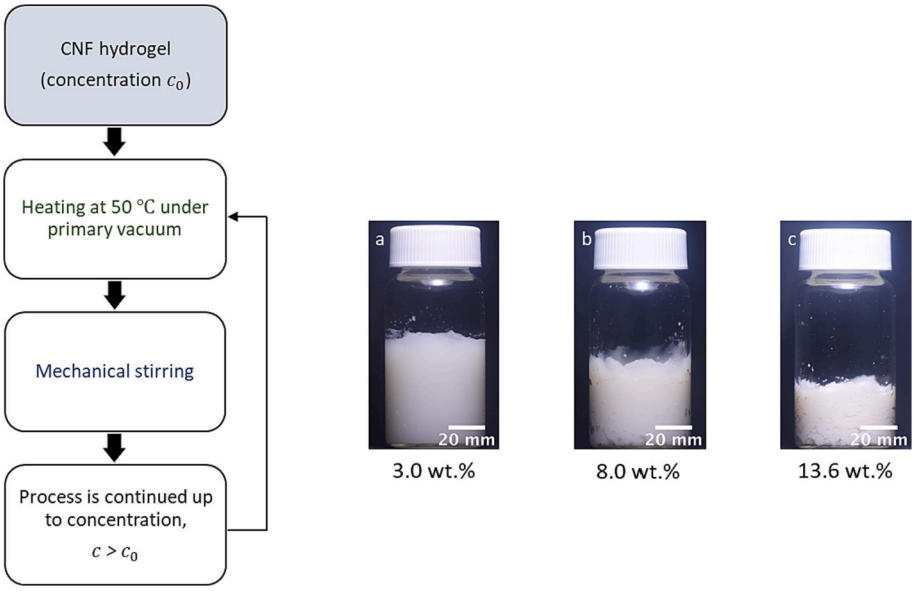

Fig. 2. Schematic representation of the methodology used to obtain CNF hydrogels at high CNF concentrations. Photographs of the CNF hydrogels at concentrations c of (a) 3.0 wt% ($\phi_f = 2$ %) and at high concentrations of (b) 8.0 wt% ($\phi_f = 5.5$ %) and (c) 13.6 wt% ($\phi_f = 9.5$ %).

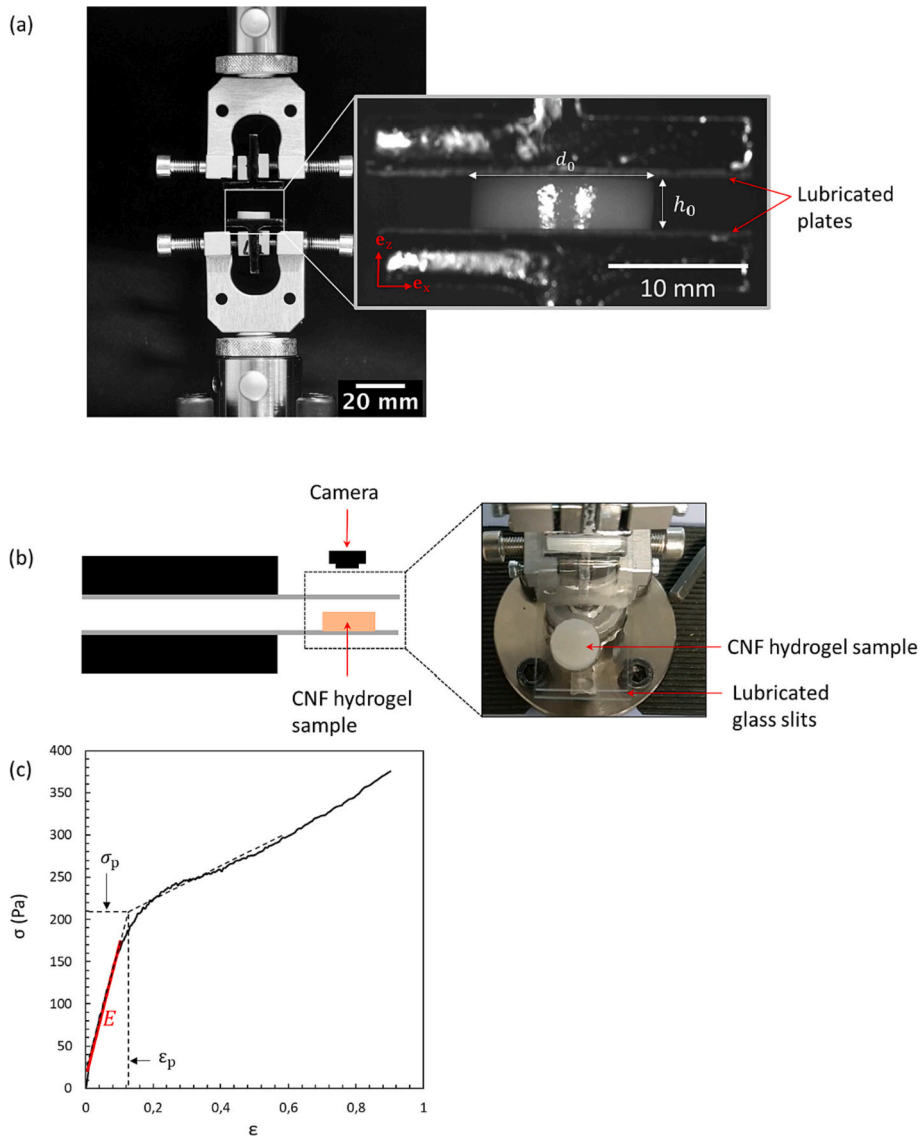

Fig. 3. (a) Photographs showing the compression setup equipped with lubricated and parallel metallic platens. (b) Scheme and photograph of the compression device equipped with lubricated and transparent glass slits, enabling the observation of the top of the samples during compression. (c) Typical stress-strain compression curve of a CNF hydrogels at $c = 3$ wt% obtained for an initial compression strain rate $\dot{\varepsilon}_0 = 0.1\ s^{-1}$.

and 13.6 wt% were compressed at a constant compression velocity of 5 mm min^{-1}. These velocities correspond to initial strain rates $\dot{\varepsilon}_0 = \left|\dot{h}/h_0\right|$ that ranged between 0.001 s^{-1} and 0.8 s^{-1}. By assuming the CNF hydrogel incompressibility, the axial compression stress $\sigma = 4|F|h/\left(\pi h_0 d_0^2\right)$ was plotted as a function of the axial compression Hencky strain $\varepsilon = |\ln(h/h_0)|$ (up to 0.9). During the tests, side views of the deformed samples were acquired using a high-frequency video camera (Fig. 3a). In addition, to better observe the in-plane flow of the samples, some compression experiments were performed between lubricated transparent glass slits that were stuck to the metallic platens as shown in Fig. 3b. Photographs showing a top view of the samples during their deformation were also taken with a video camera.

Fig. 3c shows a typical stress-strain compression curve recorded during the flow of a CNF hydrogel at a concentration ($c = 3$ wt%). From these curves, we assessed the compression modulus E of the CNF hydrogels from the linear part of the stress-strain curves. In addition, the transition stress σ_p and deformation at transition stress ε_p were also estimated from the intersection of two tangent lines, one with the initial apparent linear part and another with the strain hardening part of the stress-strain curves (Fig. 3c).

3. Results

3.1. Stress-strain curves obtained at various strain rates

Fig. 4 shows typical stress-strain curves obtained for CNF hydrogels at 3, 8 and 13.6 wt% and various compression strain rates $\dot{\varepsilon}_0$. Regardless of the CNF hydrogel concentrations and strain rates, the compression curves exhibited two distinct regimes: an apparent linear regime characterised by an apparent compression modulus E at low strain ($0 \leq \varepsilon \leq \varepsilon_p$) followed by a strain hardening or plateau-like regime ($\varepsilon \geq \varepsilon_p$). Below the strain ε_p, the compression response depended slightly on $\dot{\varepsilon}_0$. On the contrary, above ε_p, the compression response exhibited a plateau with weak or marked hardening of stress levels, depending on the applied strain rate. Astonishingly, the hardening behaviour was strengthened with decreasing the strain rate, leading to important stress levels at the end of the compression test. In addition, it is interesting to note that for all the investigated CNF contents, the stresses measured at high strain (ε

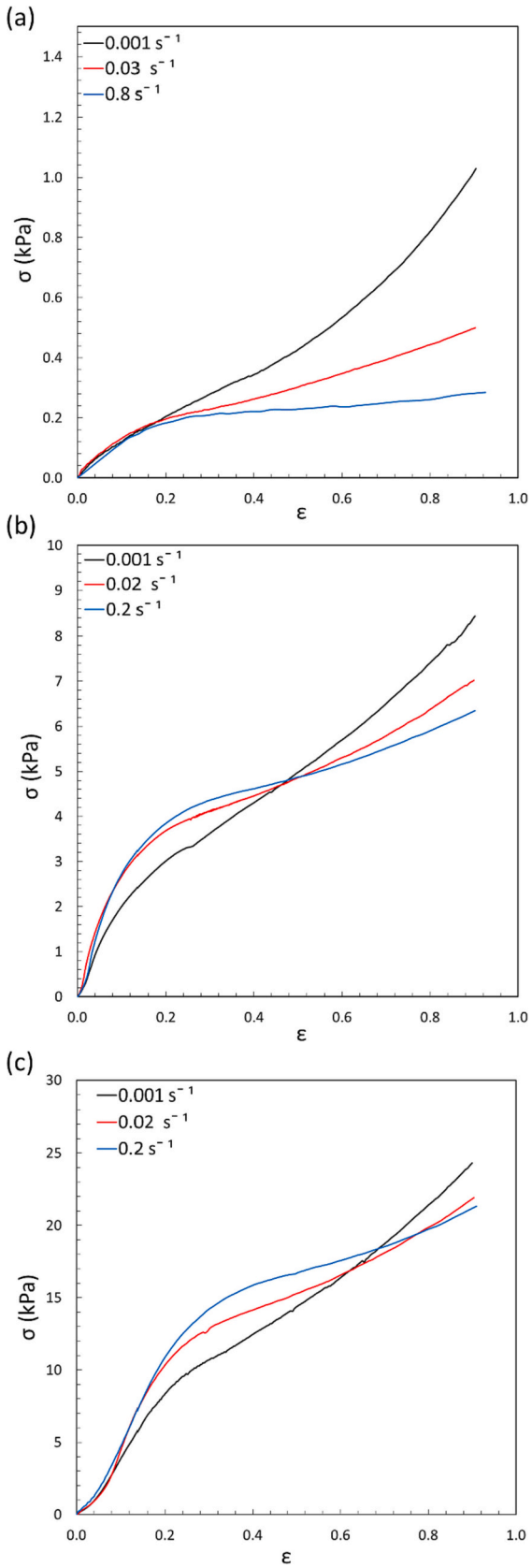

Fig. 4. Stress-strain compression curves obtained at different initial strain rates $\dot{\varepsilon}_0$ for CNF hydrogels concentrated at 3 wt% (a), 8.0 wt% (b) and 13.6 wt% (c).

> 0.7) were decreasing functions of $\dot{\varepsilon}_0$. This unusual behaviour is further illustrated in Fig. 7 for a CNF hydrogel at 3 wt%.

3.2. Stress-strain curves below ε_p

Fig. 5 shows that the apparent compression modulus E and the transition stress σ_p and strains ε_p of the CNF hydrogel at 3 wt% exhibit a high variability and slight increases for the strain rate range $0.001\ s^{-1} \leq \dot{\varepsilon}_0 \leq 0.1\ s^{-1}$. Above, these parameters exhibit lower variabilities, with still an increase for ε_p, and a decrease for E and σ_p. Fig. 6 shows that the compression modulus E and the transition stress σ_p measured when $\dot{\varepsilon}_0 = 0.2\ s^{-1}$ were power-law functions of the CNF volume fraction ϕ_f, *i.e.*, $E \propto \phi_f^{\,n}$ and $\sigma_p \propto \phi_f^{\,m}$ with $n = 2.4$ and $m = 2.7$, respectively.

3.3. Stress-strain curves above ε_p

Fig. 7 shows the evolution of the stress $\sigma_{0.7}$ measured at $\varepsilon = 0.7$ as a function of the strain rate $\dot{\varepsilon}_0$. Astonishingly, this stress exhibits a non-linear decrease with $\dot{\varepsilon}_0$. This evolution is well fitted by the power-law function $\sigma_{0.7} \propto \dot{\varepsilon}_0^{\,q}$ with $q = -0.18$. In addition, below $0.1\ s^{-1}$ that corresponded to the transition between the marked and weak strain hardening regimes (Fig. 4), it is interesting to notice that the stress $\sigma_{0.7}$ exhibits large and erratic variations. Conversely, above this point, it exhibits a lower discrepancy that is related to a more uniform flow (*cf.* Subsection 3.4).

3.4. Flow mechanisms above ε_p

The compression curves in Fig. 4 reveal that the CNF hydrogels exhibited complex in-plane equi-biaxial elongational flow properties above ε_p. Astonishingly, these curves showed that the flow stress $\sigma_{0.7}$ increased significantly with decreasing the strain rate $\dot{\varepsilon}_0$. This particular behaviour was observed for all the investigated CNF hydrogels. However, an opposite trend is commonly observed for homogeneous incompressible viscous fluids, including Newtonian, shear thinning as well as shear thickening fluids. Thus, to better understand the flow mechanisms at the origin of this particular behaviour, we performed lubricated compression tests coupled with optical visualisations on CNF hydrogels at 3 wt%.

Fig. 8 shows top and side views of a CNF hydrogel sample that were recorded during a compression test performed at $\dot{\varepsilon}_0 = 0.001\ s^{-1}$, *i.e.*, within the regime where a pronounced hardening of stress levels was observed. These photographs reveal that the samples remained practically cylindrical when $\varepsilon < \varepsilon_p \approx 0.2$, thus emphasising an homogeneous plug flow of the samples with in-plane equi-biaxial elongation. However, above ε_p, several radial cracks appeared on the outer vertical surface of the samples, emphasising an heterogeneous flow with severe damage of the CNF networks. Interestingly, these cracks were coupled with solid-liquid segregation, with noticeable migration of the hydrogel water (or a mixture of water with a low content of CNF) out of the CNF network, thereby inducing a radial gradient of the CNF concentration within the sample. This phenomenon was also associated with the formation of a whitish core area at the centre of the samples that was visible in the top views of samples. In this area, the CNF network was presumably subjected to a marked consolidation and its volume content was thus increased compared to the initial fibre volume content. Crack nucleation and propagation together with solid-liquid segregation became more and more pronounced with the increase in the compression strain.

Assuming the CNF hydrogel incompressibility, we estimated the degree of segregation ϕ_{fc}/ϕ_f between the CNF volume fraction in the core zone denoted ϕ_{fc}, *i.e.*, in the zone from which the water was expelled, and the initial CNF volume fraction ϕ_f as follows:

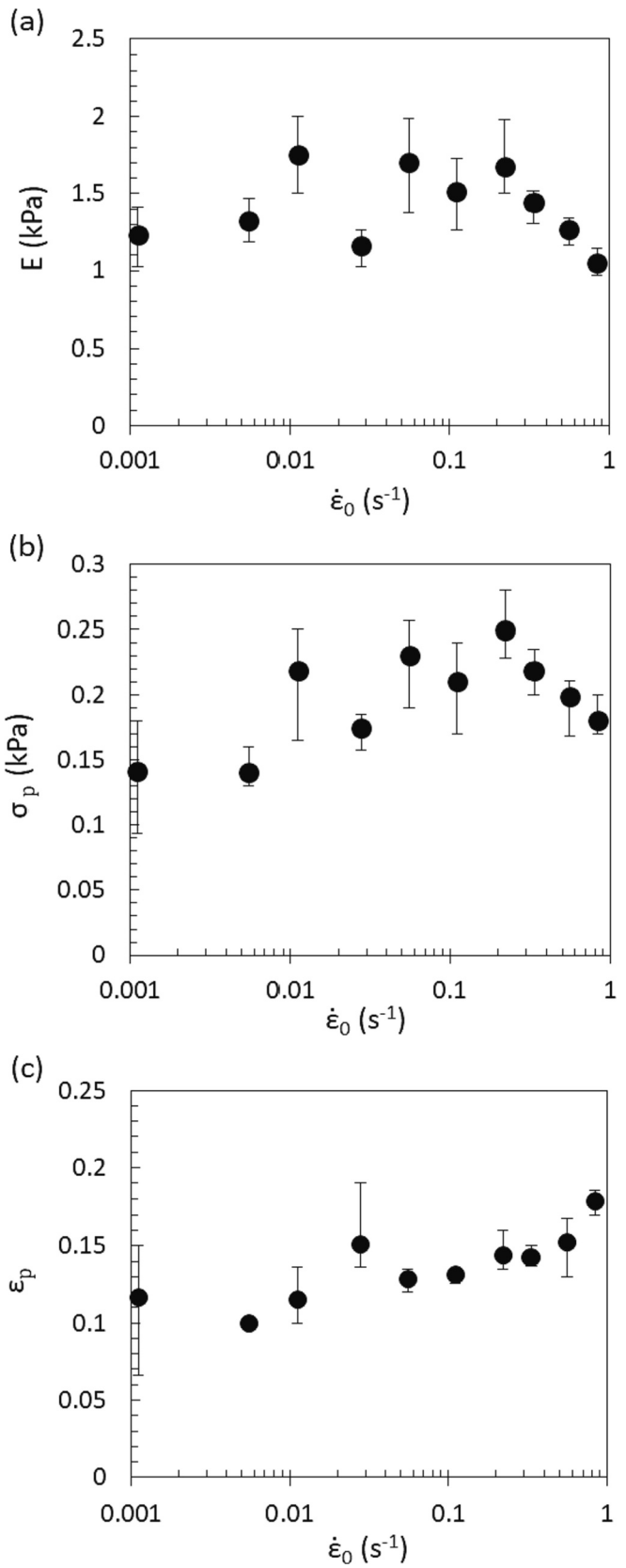

Fig. 5. Evolution of the compression modulus E (a), transition stress σ_p (b) and strain ε_p (c) as functions of the initial strain rate $\dot{\varepsilon}_0$ for a CNF hydrogel at 3 wt%.

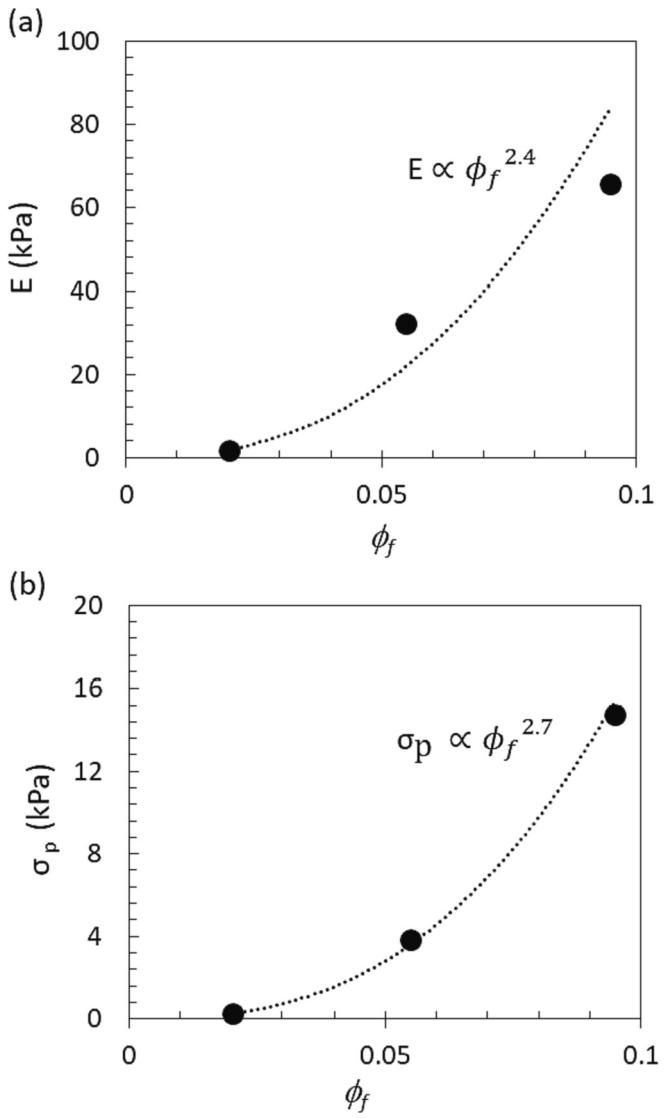

Fig. 6. Evolution of the compression modulus E (a) and the transition stress σ_p (b) as functions of the nanofibre volume fraction ϕ_f at $\dot{\varepsilon}_0 = 0.2\ s^{-1}$.

$$\frac{\phi_{fc}}{\phi_f} = \frac{h_0 S_0}{h_{0.9} S_{fc}} \tag{1}$$

where h_0 and $h_{0.9}$ are the height of the cylindrical sample measured at compression strains $\varepsilon = 0$ and $\varepsilon = 0.9$, respectively. S_0 is the initial area of the sample and S_{fc} is the area of the core zone measured at a compression strain $\varepsilon = 0.9$. Then, to measure S_{fc}, an image analysis method based on the gradient in the grey levels of the top photographs taken at an axial compression strain of 0.9 (Fig. 8) was used. The core zone was roughly identified with a thresholding operation applied on the pixels of the images with the highest grey levels (whitish zone). This operation was done manually using the Threshold function implemented in ImageJ software. Then, the area S_{fc} was measured using a pixel counting method (Schneider et al., 2012). Doing so, the ratio ϕ_{fc}/ϕ_f was slightly overestimated, since it was assumed that all CNFs were concentrated in the volume of the core zone. The low concentrated CNFs located in the greyish transition area around the central zone were not taken into account. Fig. 9 shows the evolution of the ratio ϕ_{fc}/ϕ_f as a function of the initial strain rate $\dot{\varepsilon}_0$ for a CNF hydrogel at 3 wt% as well as top views of several samples deformed at $\varepsilon = 0.9$ that were used to estimate this ratio (points 1 to 4 which are indicated in the graph). The ratio ϕ_{fc}/ϕ_f obviously exhibits a decrease with increasing the initial

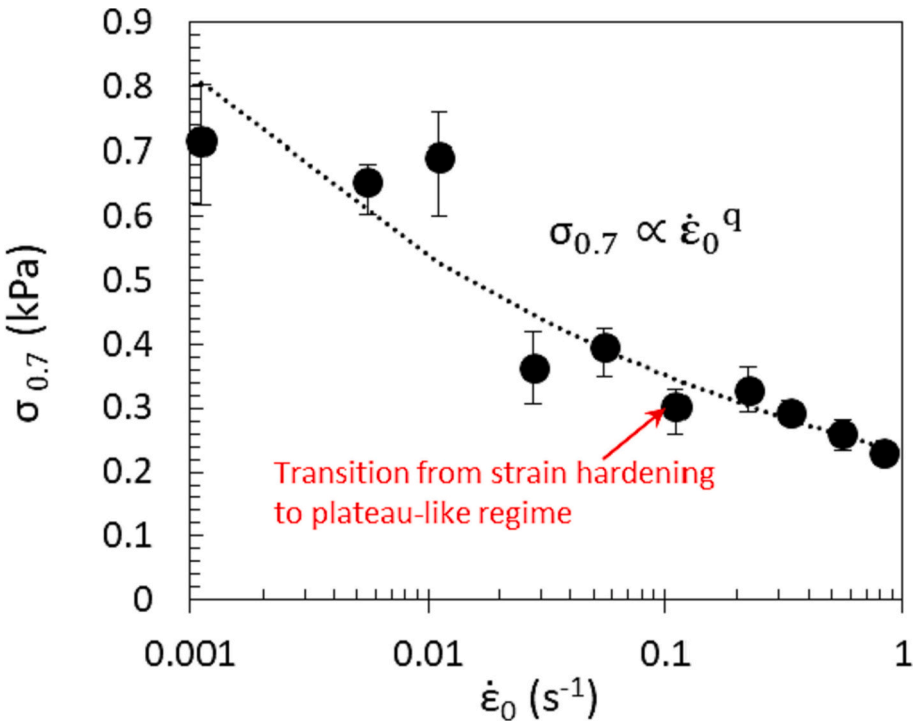

Fig. 7. Evolution of the stress $\sigma_{0.7}$ (measured at a strain $\varepsilon = 0.7$) as a function of the strain rate $\dot{\varepsilon}_0$ for a CNF hydrogel at 3 wt%.

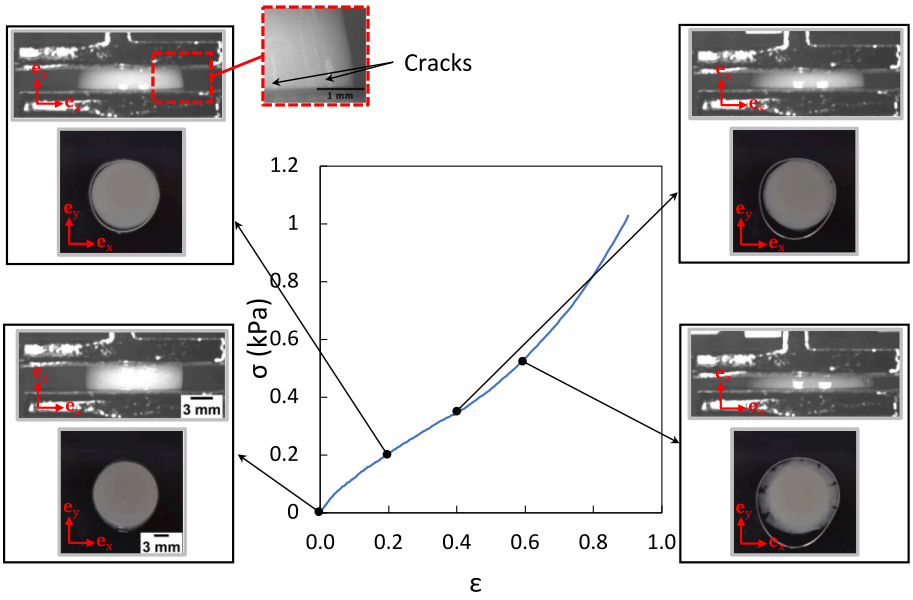

Fig. 8. Typical stress-strain curve and inset photographs showing the top and side views of a CNF hydrogel sample at 3 wt% during a compression performed at $\dot{\varepsilon}_0 = 0.001\ s^{-1}$.

strain rate $\dot{\varepsilon}_0$. Indeed, for the lowest initial strain rates ($\dot{\varepsilon}_0 \leq 0.01\ s^{-1}$), ϕ_{fc}/ϕ_f is approximately equal to 2–2.3, showing that a large quantity of water was expelled from the samples. As underlined in the previous paragraph, this phenomenon is also associated to a pronounced consolidation of the CNF phase within the CNF hydrogels during compression. In addition, for initial strain rates $\dot{\varepsilon}_0 > 0.01\ s^{-1}$, ϕ_{fc}/ϕ_f progressively reaches the value of one, showing that the deformation of the samples was more and more homogeneous as the strain rate $\dot{\varepsilon}_0$ was increased, so that the flow of the CNF hydrogels tended to be one-phase and incompressible for the highest investigated compression strain rate of $0.5\ s^{-1}$.

The aforementioned flow mechanisms were also presumably at the origin of the complex rheology behaviour shown in Fig. 4b, c for CNF hydrogels at higher concentrations.

4. Discussion

The previous results show the critical effect of the compression strain rate $\dot{\varepsilon}_0$ on the compression response of the studied enzymatic CNF hydrogels. At the lowest compression strain rates, the stress-strain compression response exhibited (i) a large discrepancy and (ii) a two-phase flow with liquid migration, cracks of the fibrous network and

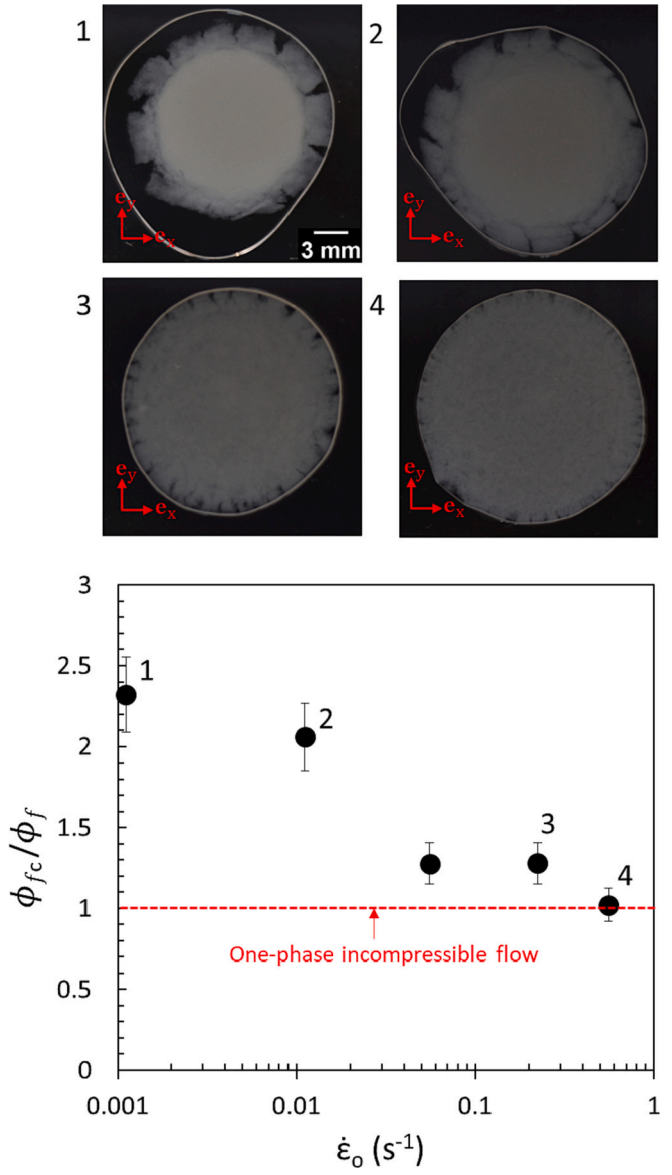

Fig. 9. Evolution of the ratio ϕ_{fc}/ϕ_f as a function of $\dot{\varepsilon}_0$ obtained from several samples of CNF hydrogel at 3 wt% deformed at a compression strain $\varepsilon = 0.9$. Note that these values were obtained from the averaging of three measurements. The photographs show top views of the deformed samples corresponding to the numbers indicated in the graph.

pronounced hardening of stress levels. Concerning point (i), the observed discrepancy could arise from the heterogeneous structure of enzymatic CNF hydrogels: it has often been reported that these hydrogels exhibit flocculated mesostructures due to dominant van der Waals colloidal attractive forces between nanofibres. For point (ii), the observed hardening is linked with a consolidation of the CNF networks in the centre of the samples, *i.e.*, a compression-induced increase of the volume fraction of CNF in this zone, as emphasised in Fig. 9. Such a consolidation could result from the in-plane flow of water through the networks of CNF and, more probably, through the networks of CNF flocs as well as through the observed opening cracks. On the opposite, for the largest investigated strain rate, the observed flow was practically a one-phase and incompressible flow with small radial cracks that appeared at large compression strains. Furthermore, the compression response of the investigated CNF hydrogels was less scattered with a weak or moderate hardening of stress levels. This behaviour could be related to the disentanglement of the CNFs together with their reorientation perpendicular to the compression axis (Laurencin et al., 2019) and/or the disaggregation of CNF flocs. For this strain rate, the interstitial pressure of water should reach sufficient high values to promote these mechanisms and to restrain fluid migration. Thus, by progressively increasing the compression strain rate, the marked two-phase flow regime evolved towards a one-phase flow regime with less consolidation and segregation, leading presumably to the establishment of homogeneous in-plane deformation of the CNF networks and CNF flocs. This mechanism could also explain the decrease in the scattering of the results. It could also be at the origin of CNF volume fractions that remained closer and closer to the initial CNF volume fraction with the increase in the compression strain rate. This could explain the slight decrease of the compression modulus E and transition stress σ_p observed for compression strain rates that were above the aforementioned transition compression strain rate that corresponds to the occurrence of the plateau-like regime.

It is important to notice that similar compression behaviour, *i.e.*, with fluid-fibre segregation and fibre network consolidation at low compression rates and homogeneous flow at higher compression strain rates, has already been reported for granular suspensions, *i.e.*, cement mortars (Cardoso et al., 2009), fibre-reinforced suspensions such as fibre-reinforced mortars (Chalencon et al., 2016) or fibre-reinforced polymer composites (Orgéas et al., 2008), that were subjected to lubricated compression experiments. This complex behaviour was shown to be governed by the suspending fluid viscosity, the fibre network connectivity and permeability (Orgéas et al., 2015).

For the nearly one-phase and homogeneous flow conditions, keeping in mind that the investigated strain rates remained relatively low, the transition stresses σ_p could be reasonably associated to a compression yield stress σ_Y and thus compared with shear yield stresses available in the literature for similar CNF hydrogels. For that purpose, the shear yield stress τ_Y of the tested CNF hydrogels was deduced from the compression yield stress σ_Y using the Von Mises criterion (Ovarlez et al., 2010), *i.e.*, $\tau_Y = \sigma_Y/\sqrt{3}$. Hence, Fig. 10 shows the evolution of the as-calculated yield stress τ_Y as a function of the fibre volume fraction ϕ_f for the studied CNF hydrogels as well as yield stress values obtained from the literature for several mechanically and enzymatically treated CNF hydrogels that exhibited flocculated mesostructures (Koponen, 2020). A

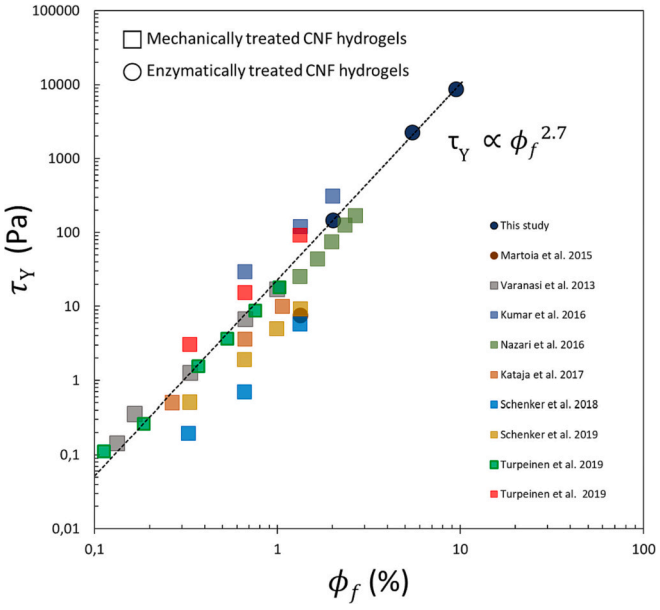

Fig. 10. Evolution of the shear yield stress τ_Y as a function of the CNF volume fraction ϕ_f for the CNF hydrogels investigated in this study and for mechanically and enzymatically treated CNF hydrogels reported in (Koponen, 2020). Dashed line: power law function identified in this study.

remarkable result is that the evolution of all reported shear yield stresses τ_Y reasonably follows the power-law function that has been identified in Subsection 3.2. However, the shear yield stress τ_Y exhibits a large scattering between these experiments. Its origin can be related to the differences in the CNF morphology (slenderness, tortuosity) (Bennington et al., 1990; Sanchez-Salvador et al., 2020; Varanasi et al., 2013) the CNF physico-chemical surface properties (surface charge density) (Mendoza et al., 2018), the CNF mechanical properties (CNF longitudinal moduli, presence of defects) as well as in the formation of microstructures (differences in CNF orientation (Martoïa et al., 2016; Rosén et al., 2020)) and mesostructures (variations in size and shape of CNF flocs (Karppinen et al., 2012; Martoïa et al., 2015; Saarikoski et al., 2012)) and the physico-chemical properties of the suspending fluid (*e.g.*, ionic force (Sim et al., 2015)). The measurements of the shear yield stress τ_Y can also be affected by heterogeneous flow conditions (*e.g.*, wall-slippage, shear wall depletion, shear banding) that are known to arise during this type of experiments (Martoïa et al., 2015; Nechyporchuk et al., 2014; Saarinen et al., 2014).

5. Conclusion

Original lubricated compression tests were performed to probe the in-plane equi-biaxial elongational flow properties of concentrated and highly concentrated enzymatic CNF hydrogels. The compression curves of CNF hydrogels exhibited two distinct regimes, regardless of the CNF concentration. First, an initial linear regime characterised by an apparent compression modulus appears at low strain. This regime was followed by a plateau with weak or marked hardening of stress levels. Photographs of the samples that were acquired during compression revealed that the pronounced hardening observed at low strain rates was associated to fluid segregation and CNF network consolidation, *i.e.*, to the development of a two-phase flow behaviour of the CNF hydrogels. For the highest strain rates, the hardening was restrained and photographs proved the occurrence of a one-phase and incompressible flow. Furthermore, by estimating from these measurements a shear yield stress, we showed that the measured yield stress was close to values reported in the literature for a wide range of mechanically and enzymatically treated CNF hydrogels with classical and moderate CNF concentrations. Interestingly, most of the literature data followed the same scaling law with the nanofibre content, and also our data obtained in the concentrated and hyper-concentrated regimes.

Processing highly concentrated CNF hydrogels is a desired solution to reduce logistics costs and drying energy and to produce CNF-based materials with good dimensional stability. However, to fully exploit the remarkable intrinsic properties of CNFs and thus to manufacture CNF-based materials with optimised end-use properties, it is crucial to build or feed 3D tensorial rheological models for the prediction of the rheological behaviour and the flow-induced microstructures of CNF hydrogels in situations that are representative of industrial processing conditions. In the case of one-phase and incompressible flow situations, the rheology of concentrated and highly concentrated CNF hydrogels could be modelled using existing phenomenological elastoviscoplastic (Fraggedakis et al., 2016) or multiscale (Bounoua et al., 2016; Martoïa et al., 2016) models. However, the prediction of the two-phase flow behaviour of the CNF hydrogels during material forming processes constitutes a challenging task that is required to optimise the processing conditions (*e.g.*, applied stress, flow rate, tool geometry, *etc.*) and limit the formation of defects (*e.g.*, the spatial variations in CNF contents, formation of pores, heterogeneous CNF orientations, *etc.*) in CNF-based materials. Various two-phase modelling approaches are reported in the literature (Orgéas et al., 2015) and could be used for that purpose. However, these approaches often required the knowledge of microstructure descriptors such as the fibre network connectivity and permeability that are up to now unknown for enzymatic CNF and/or CNF floc networks.

Data availability

Data will be made available on request.

Acknowledgments

This research was supported by IDEX Université Grenoble Alpes and Labex Tec21. The authors gratefully acknowledge LabEX Tec 21 and the research site of INSA Lyon at Oyonnax for administrative and technical support. The laboratories 3SR is part of the LabEx Tec 21 (Investissements d'Avenir-grant agreement n°ANR-11-LABX-0030) and the Carnot Institute Polynat (n° ANR16-CARN-0025). The authors also thank J.-L. Putaux (CERMAV) for his support in the experiments performed using the transmission electron microscope.

References

Bennington, C. P. J., Kerekes, R. J., & Grace, J. R. (1990). The yield stress of fibre suspensions. *The Canadian Journal of Chemical Engineering, 68*(5), 748–757. https://doi.org/10.1002/cjce.5450680503

Bounoua, S., Lemaire, E., Férec, J., Ausias, G., & Kuzhir, P. (2016). Shear-thinning in concentrated rigid fiber suspensions: Aggregation induced by adhesive interactions. *Journal of Rheology, 60*(6), 1279–1300. https://doi.org/10.1122/1.4965431

Cardoso, F. A., John, V. M., & Pileggi, R. G. (2009). Rheological behavior of mortars under different squeezing rates. *Cement and Concrete Research, 39*(9), 748–753. https://doi.org/10.1016/j.cemconres.2009.05.014

Chalencon, F., Orgéas, L., Dumont, P. J. J., Foray, G., Cavaillé, J.-Y., Maire, E., & Rolland du Roscoat, S. (2010). Lubricated compression and X-ray microtomography to analyse the rheology of a fibre-reinforced mortar. *Rheologica Acta, 49*(3), 221–235. https://doi.org/10.1007/s00397-009-0393-5

Chalencon, F., Dumont, P. J. J., Orgéas, L., Foray, G., Cavaillé, J.-Y., & Maire, E. (2016). Homogeneous and heterogeneous rheology and flow-induced microstructures of a fresh fiber-reinforced mortar. *Cement and Concrete Research, 82*, 130–141. https://doi.org/10.1016/j.cemconres.2015.12.012

Cheng, Q., Wang, S., & Harper, D. P. (2009). Effects of process and source on elastic modulus of single cellulose fibrils evaluated by atomic force microscopy. *Composites Part A: Applied Science and Manufacturing, 40*(5), 583–588. https://doi.org/10.1016/j.compositesa.2009.02.011

Dimic-Misic, K., Maloney, T., Liu, G., & Gane, P. (2017). Micro nanofibrillated cellulose (MNFC) gel dewatering induced at ultralow-shear in presence of added colloidally-unstable particles. *Cellulose, 24*(3), 1463–1481. https://doi.org/10.1007/s10570-016-1181-x

Dufresne, A. (2017). *Nanocellulose: From nature to high performance tailored materials.* Walter de Gruyter GmbH & Co KG.

Fraggedakis, D., Dimakopoulos, Y., & Tsamopoulos, J. (2016). Yielding the yield stress analysis: A thorough comparison of recently proposed elasto-visco-plastic (EVP) fluid models. *Journal of Non-Newtonian Fluid Mechanics, 236*, 104–122. https://doi.org/10.1016/j.jnnfm.2016.09.00

Gómez, H. C., Serpa, A., Velásquez-Cock, J., Gañán, P., Castro, C., Vélez, L., & Zuluaga, R. (2016). Vegetable nanocellulose in food science: A review. *Food Hydrocolloids, 57*, 178–186. https://doi.org/10.1016/j.foodhyd.2016.01.023

Guiraud, O., Dumont, P. J. J., Orgéas, L., & Favier, D. (2012). Rheometry of compression moulded fibre-reinforced polymer composites: Rheology, compressibility, and friction forces with mould surfaces. *Composites Part A: Applied Science and Manufacturing, 43*(11), 2107–2119.

Gupta, S., Martoïa, F., Orgéas, L., & Dumont, P. J. J. (2018). Ice-templated porous nanocellulose-based materials: Current progress and opportunities for materials engineering. *Applied Sciences, 8*(12), 2463. https://doi.org/10.3390/app8122463

Henriksson, M., Henriksson, G., Berglund, L. A., & Lindström, T. (2007). An environmentally friendly method for enzyme-assisted preparation of microfibrillated cellulose (MFC) nanofibers. *European Polymer Journal, 43*(8), 3434–3441. https://doi.org/10.1016/j.eurpolymj.2007.05.038

Hubbe, M. A., Tayeb, P., Joyce, M., Tyagi, P., Kehoe, M., Dimic-Misic, K., & Pal, L. (2017). Rheology of nanocellulose-rich aqueous suspensions: A review. *BioResources, 12*(4). https://doi.org/10.15376/biores.12.4.9556-9661, 9556–9661–9661.

Isogai, A., Saito, T., & Fukuzumi, H. (2011). TEMPO-oxidized cellulose nanofibers. *Nanoscale, 3*(1), 71–85. https://doi.org/10.1039/C0NR00583E

Jaiswal, A. K., Kumar, V., Khakalo, A., Lahtinen, P., Solin, K., Pere, J., & Toivakka, M. (2021). Rheological behavior of high consistency enzymatically fibrillated cellulose suspensions. *Cellulose, 28*(4), 2087–2104. https://doi.org/10.1007/s10570-021-03688-y

Karppinen, A., Saarinen, T., Salmela, J., Laukkanen, A., Nuopponen, M., & Seppälä, J. (2012). Flocculation of microfibrillated cellulose in shear flow. *Cellulose, 19*(6), 1807–1819. https://doi.org/10.1007/s10570-012-9766-5

Kim, H. C., Kim, D., Lee, J. Y., Zhai, L., & Kim, J. (2019). Effect of wet spinning and stretching to enhance mechanical properties of cellulose nanofiber filament. *International Journal of Precision Engineering and Manufacturing-Green Technology, 6*(3), 567–575. https://doi.org/10.1007/s40684-019-00070-z

Klemm, D., Cranston, E. D., Fischer, D., Gama, M., Kedzior, S. A., Kralisch, D., Kramer, F., Kondo, T., Lindström, T., Nietzsche, S., Petzold-Welcke, K., & Rauchfuß, F. (2018). Nanocellulose as a natural source for groundbreaking applications in materials

science: Today's state. *Materials Today, 21*(7), 720–748. https://doi.org/10.1016/j.mattod.2018.02.001

Koponen, A. I. (2020). The effect of consistency on the shear rheology of aqueous suspensions of cellulose micro- and nanofibrils: A review. *Cellulose, 27*(4), 1879–1897. https://doi.org/10.1007/s10570-019-02908-w

Laurencin, T., Laure, P., Orgéas, L., Dumont, P. J. J., Silva, L., & Rolland du Roscoat, S. (2019). Fibre kinematics in dilute non-newtonian fibre suspensions during confined and lubricated squeeze flow: Direct numerical simulation and analytical modelling. *Journal of Non-Newtonian Fluid Mechanics, 273*, Article 104187. https://doi.org/10.1016/j.jnnfm.2019.104187

Lavoine, N., Desloges, I., Dufresne, A., & Bras, J. (2012). Microfibrillated cellulose – its barrier properties and applications in cellulosic materials: A review. *Carbohydrate Polymers, 90*(2), 735–764. https://doi.org/10.1016/j.carbpol.2012.05.026

Le Corre, S., Orgéas, L., Favier, D., Tourabi, A., Maazouz, A., & Venet, C. (2002). Shear and compression behaviour of sheet moulding compounds. *Composites Science and Technology, 62*(4), 571–577. https://doi.org/10.1016/S0266-3538(01)00151-8

Li, A., Xu, D., Luo, L., Zhou, Y., Yan, W., Leng, X., Dai, D., Zhou, Y., Ahmad, H., Rao, J., & Fan, M. (2021). Overview of nanocellulose as additives in paper processing and paper products. *Nanotechnology Reviews, 10*(1), 264–281. https://doi.org/10.1515/ntrev-2021-0023

Liu, W., Liu, K., Du, H., Zheng, T., Zhang, N., Xu, T., Pang, B., Zhang, X., Si, C., & Zhang, K. (2022). Cellulose nanopaper: Fabrication, functionalization, and applications. *Nano-Micro Letters, 14*(1), 104. https://doi.org/10.1007/s40820-022-00849-x

Lundahl, M. J., Klar, V., Wang, L., Ago, M., & Rojas, O. J. (2017). Spinning of cellulose nanofibrils into filaments: A review. *Industrial & Engineering Chemistry Research, 56*(1), 8–19. https://doi.org/10.1021/acs.iecr.6b04010

Lundahl, M. J., Berta, M., Ago, M., Stading, M., & Rojas, O. J. (2018). Shear and extensional rheology of aqueous suspensions of cellulose nanofibrils for biopolymer-assisted filament spinning. *European Polymer Journal, 109*, 367–378. https://doi.org/10.1016/j.eurpolymj.2018.10.006

Martoïa, F., Perge, C., Dumont, P. J. J., Orgéas, L., Fardin, M. A., Manneville, S., & Belgacem, M. N. (2015). Heterogeneous flow kinematics of cellulose nanofibril suspensions under shear. *Soft Matter, 11*(24), 4742–4755. https://doi.org/10.1039/C5SM00530B

Martoïa, F., Dumont, P. J. J., Orgéas, L., Belgacem, M. N., & Putaux, J.-L. (2016). Micro-mechanics of electrostatically stabilized suspensions of cellulose nanofibrils under steady state shear flow. *Soft Matter, 12*(6), 1721–1735. https://doi.org/10.1039/C5SM02310F

Meeten, G. (2002). Constant-force squeeze flow of soft solids. *Rheologica Acta, 41*(6), 557–566. https://doi.org/10.1007/s00397-002-0241-3

Meftahi, A., Samyn, P., Geravand, S. A., Khajavi, R., Alibkhshi, S., Bechelany, M., & Barhoum, A. (2022). Nanocelluloses as skin biocompatible materials for skincare, cosmetics, and healthcare: Formulations, regulations, and emerging applications. *Carbohydrate Polymers, 278*, Article 118956. https://doi.org/10.1016/j.carbpol.2021.118956

Mendoza, L., Gunawardhana, T., Batchelor, W., & Garnier, G. (2018). Effects of fibre dimension and charge density on nanocellulose gels. *Journal of Colloid and Interface Science, 525*, 119–125. https://doi.org/10.1016/j.jcis.2018.04.077

Missoum, K., Martoïa, F., Belgacem, M. N., & Bras, J. (2013). Effect of chemically modified nanofibrillated cellulose addition on the properties of fiber-based materials. *Industrial Crops and Products, 48*, 98–105. https://doi.org/10.1016/j.indcrop.2013.04.013

Moberg, T., Rigdahl, M., Stading, M., & Levenstam Bragd, E. (2014). Extensional viscosity of microfibrillated cellulose suspensions. *Carbohydrate Polymers, 102*, 409–412. https://doi.org/10.1016/j.carbpol.2013.11.041

Moon, R. J., Martini, A., Nairn, J., Simonsen, J., & Youngblood, J. (2011). Cellulose nanomaterials review: Structure, properties and nanocomposites. *Chemical Society Reviews, 40*(7), 3941–3994. https://doi.org/10.1039/C0CS00108B

Nechyporchuk, O., Belgacem, M. N., & Pignon, F. (2014). Rheological properties of micro-/nanofibrillated cellulose suspensions: Wall-slip and shear banding phenomena. *Carbohydrate Polymers, 112*, 432–439. https://doi.org/10.1016/j.carbpol.2014.05.092

Nechyporchuk, O., Belgacem, M. N., & Pignon, F. (2015). Concentration effect of TEMPO-oxidized nanofibrillated cellulose aqueous suspensions on the flow instabilities and small-angle X-ray scattering structural characterization. *Cellulose, 22*(4), 2197–2210. https://doi.org/10.1007/s10570-015-0640-0

Nechyporchuk, O., Belgacem, M. N., & Bras, J. (2016). Production of cellulose nanofibrils: A review of recent advances. *Industrial Crops and Products, 93*, 2–25. https://doi.org/10.1016/j.indcrop.2016.02.016

Orgéas, L., Dumont, P. J. J., Michaud, V., & Favier, D. (2008). Separation of the polymer matrix and the fibrous reinforcement during compression moulding of glass mat thermoplastics (GMT). *International Journal of Material Forming, 1*(1), 929–932. https://doi.org/10.1007/s12289-008-0249-z

Orgéas, L., Dumont, P., & Corre, S. L. (2015). 5—Rheology of highly concentrated fiber suspensions. In F. Chinesta, & G. Ausias (Eds.), *Rheology of non-spherical particle suspensions* (pp. 119–166). Elsevier. https://doi.org/10.1016/B978-1-78548-036-2.50005-8.

Ovarlez, G., Barral, Q., & Coussot, P. (2010). Three-dimensional jamming and flows of soft glassy materials. *Nature Materials, 9*(2), 115–119. https://doi.org/10.1038/nmat2615

Pääkkö, M., Ankerfors, M., Kosonen, H., Nykänen, A., Ahola, S., Österberg, M., Ruokolainen, J., Laine, J., Larsson, P. T., Ikkala, O., & Lindström, T. (2007). Enzymatic hydrolysis combined with mechanical shearing and high-pressure homogenization for nanoscale cellulose fibrils and strong gels. *Biomacromolecules, 8*(6), 1934–1941. https://doi.org/10.1021/bm061215p

Rantanen, J. J., Dimic-Misic, K., Pirttiniemi, J., Kuosmanen, P., & Maloney, T. C. (2015). Forming and dewatering of a microfibrillated cellulose composite paper. *BioResources, 10*(2), 3492–3506.

Rosén, T., Wang, R., Zhan, C., He, H., Chodankar, S., & Hsiao, B. S. (2020). Cellulose nanofibrils and nanocrystals in confined flow: Single-particle dynamics to collective alignment revealed through scanning small-angle x-ray scattering and numerical simulations. *Physical Review E, 101*(3), Article 032610. https://doi.org/10.1103/PhysRevE.101.032610

Saarikoski, E., Saarinen, T., Salmela, J., & Seppälä, J. (2012). Flocculated flow of microfibrillated cellulose water suspensions: An imaging approach for characterisation of rheological behaviour. *Cellulose, 19*(3), 647–659. https://doi.org/10.1007/s10570-012-9661-0

Saarinen, T., Haavisto, S., Sorvari, A., Salmela, J., & Seppälä, J. (2014). The effect of wall depletion on the rheology of microfibrillated cellulose water suspensions by optical coherence tomography. *Cellulose, 21*(3), 1261–1275. https://doi.org/10.1007/s10570-014-0187-5

Saito, T., Kimura, S., Nishiyama, Y., & Isogai, A. (2007). Cellulose nanofibers prepared by TEMPO-mediated oxidation of native cellulose. *Biomacromolecules, 8*(8), 2485–2491. https://doi.org/10.1021/bm0703970

Sanchez-Salvador, J. L., Monte, M. C., Batchelor, W., Garnier, G., Negro, C., & Blanco, A. (2020). Characterizing highly fibrillated nanocellulose by modifying the gel point methodology. *Carbohydrate Polymers, 227*, Article 115340. https://doi.org/10.1016/j.carbpol.2019.115340

Schneider, C. A., Rasband, W. S., & Eliceiri, K. W. (2012). NIH image to ImageJ: 25 years of image analysis. *Nature Methods, 9*(7), 671–675. https://doi.org/10.1038/nmeth.2089

Sim, K., Lee, J., Lee, H., & Youn, H. J. (2015). Flocculation behavior of cellulose nanofibrils under different salt conditions and its impact on network strength and dewatering ability. *Cellulose, 22*(6), 3689–3700. https://doi.org/10.1007/s10570-015-0784-y

Sinquefield, S., Ciesielski, P. N., Li, K., Gardner, D. J., & Ozcan, S. (2020). Nanocellulose dewatering and drying: Current state and future perspectives. *ACS Sustainable Chemistry & Engineering, 8*(26), 9601–9615. https://doi.org/10.1021/acssuschemeng.0c01797

Varanasi, S., He, R., & Batchelor, W. (2013). Estimation of cellulose nanofibre aspect ratio from measurements of fibre suspension gel point. *Cellulose, 20*(4), 1885–1896. https://doi.org/10.1007/s10570-013-9972-9

Wang, Q., Yao, Q., Liu, J., Sun, J., Zhu, Q., & Chen, H. (2019). Processing nanocellulose to bulk materials: A review. *Cellulose, 26*(13), 7585–7617. https://doi.org/10.1007/s10570-019-02642-3